

***Ab initio* structural, elastic, and vibrational properties of carbon nanotubes**

Daniel Sánchez-Portal, Emilio Artacho, and José M. Soler

Departamento de Física de la Materia Condensada and Instituto Nicolás Cabrera, C-III, Universidad Autónoma de Madrid, 28049 Madrid, Spain

Angel Rubio

Departamento de Física Teórica, Universidad de Valladolid, 47011 Valladolid, Spain

Pablo Ordejón

Departamento Física, Universidad de Oviedo, 33007 Oviedo, Spain

(Received 11 November 1998)

A study based on *ab initio* calculations is presented on the structural, elastic, and vibrational properties of single-wall carbon nanotubes with different radii and chiralities. These properties are obtained using an implementation of pseudopotential-density-functional theory, which allows calculations on systems with a large number of atoms per cell. Different quantities are monitored versus tube radius. The validity of expectations based on graphite is explored down to small radii, where some deviations appear related to the curvature-induced rehybridization of the carbon orbitals. Young moduli are found to be very similar to graphite and do not exhibit a systematic variation with either the radius or the chirality. The Poisson ratio also retains graphitic values except for a possible slight reduction for small radii. It shows, however, chirality dependence. The behavior of characteristic phonon branches as the breathing mode, twistons, and high-frequency optic modes, is also studied, the latter displaying a small chirality dependence at the top of the band. The results are compared with the predictions of the simple zone-folding approximation. Except for the known deficiencies of the zone-folding procedure in the low-frequency vibrational regions, it offers quite accurate results, even for relatively small radii. [S0163-1829(99)02919-7]

I. INTRODUCTION

Carbon nanotubes have excited a considerable interest in the condensed-matter and materials research communities in the last few years, and much experimental and theoretical work has been devoted to them as prototype of one-dimensional ordered systems with promising technological applications.¹ Electronic transport in conducting nanotubes is one of the issues that has attracted more attention, especially after the developments that made possible the synthesis of large quantities of single-wall nanotubes (SWNT) forming crystalline ropes.^{2,3} Experiments showed a peculiar metallic behavior above 35 K, which was understood in terms of the coupling between the conduction electrons and long wavelength twistons, i.e., torsional-shape vibrations.⁴ The quantitative understanding and characterization of this and other related phenomena require the detailed knowledge of both the structure and the vibrations of these tubes.

The structure of carbon nanotubes is qualitatively well known through the simple construction of rolling a perfect graphene sheet, where only one parameter is to be determined: the lattice parameter or a bond length. The symmetry of the tubes is less restrictive than in graphite and several parameters are needed to determine completely the structure. Among other things, these parameters define the differences between inequivalent bonds, which condition the position of the Fermi surface in the conducting armchair tubes. It is very difficult to obtain direct experimental information for the structure, and very little theoretical information has been given so far.⁵⁻⁷

Besides possible nanotechnological applications, carbon

nanotubes are promising candidates for composite materials where their low weight and very high Young modulus can be of use. Their elastic properties have thus received considerable attention as well. The nanotube's unusual strength arises from a combination of high stiffness and an extraordinary flexibility and resistance to fracture.⁸⁻¹⁰ The Young modulus of SWNT has been measured from the amplitude of their thermal vibrations¹¹ and by measuring the bending force of a pinned nanotube by an atomic-force microscope.¹² The experimental results give a Young modulus in the range of one TPa, similar to the one of graphite when pulled parallel to the sheets, but the experimental uncertainty is quite high. There is also a dispersion of theoretical values^{8,9,13-16} in the literature for this quantity corresponding to different approximations, but also to different definitions of the effective sectional area.

Raman experiments¹⁷ offer valuable information for the vibrations of ropes of single-wall armchair (n,n) tubes. The use of resonant Raman scattering¹⁸ allows us to discriminate the vibrations stemming from tubes of different diameters by looking mainly at the A_{1g} breathing mode that exhibit a strong dependence on tube diameter. Furthermore, the optical E_{2g} phonon peak shows size-dependent multiple splittings that are nearly independent of chirality and can be used to determine the tube diameter.¹⁹ Raman scattering, however, is limited to the neighborhood of the center of the Brillouin zone, and additional selection rules limit the number of vibrations detectable to seven per tube type. The theoretical characterization of the vibrational modes can complement this knowledge allowing to correlate tube diameter to a specific vibrational frequency. There is theoretical information

available based on empirical force constants¹⁷ and tight-binding Hamiltonians,^{20,21} but a first-principles theoretical reference is still lacking²² (except for the breathing mode⁷).

The strong similarity of the chemistry of carbon nanotubes to graphite allows theoretical analyses to be done based on empirical methodologies imported from studies on graphite. They range from the direct zone folding²³ of the results for graphite to the quantum-mechanical studies based on tight-binding Hamiltonians fitted to graphite properties.^{20,21,24} Effective interatomic potentials,¹³ force-constant models,¹⁵ or nonorthogonal tight-binding¹⁶ have also been tried. The performance of the different techniques varies, from the qualitative picture offered by zone folding, with intrinsic deficiencies for low frequencies, to the very quantitative results of tight-binding approaches. The curvature of the tubes, however, disturbs the chemistry in a way that can cause the deviation, from the graphite-based description, for narrow tubes. Zone folding and force constants neglect curvature altogether. Model potentials can only account for the different distances among the atoms. Tight binding captures part of the chemical strain through the geometry dependence of its electronic matrix elements, even though their absolute value depend on the electronic structure of graphite. It is then important to be able to compute the different properties for any tube radius using a tool that does not depend on a fit to graphitic properties, so as to study the narrow-tube properties with the same degree of accuracy as the wide ones.

In the present paper we present an *ab initio* study of the structural, elastic, and vibrational properties of single-wall carbon nanotubes for different diameters and chiralities to address the points mentioned above. The behavior of the different properties is monitored versus tube radius, and the performance of the different approximations used in the literature is studied to ascertain on their different ranges of applicability. Section II describes the methodological details. The results and discussion are presented in Sec. III, to finish with the concluding remarks in Sec. IV.

II. COMPUTATIONAL SCHEME

The first-principles scheme used in this study was described in detail elsewhere,²⁵ where it was already applied and tested on large fullerene molecules. It is based on the local-density approximation (LDA) to density-functional theory.²⁶ Core electrons are replaced by nonlocal, normconserving pseudopotentials,²⁷ whereas valence electrons are described within the linear combination of atomic orbitals (LCAO) approximation. In this paper we have used a minimal basis set of one *s* and three *p* orbitals per carbon atom. Although this basis is certainly not complete, it provides a sufficiently accurate description of the systems and effects that we intend to study.

The radial shape of the atomic basis functions is chosen according to the prescription of Sankey and Niklewski.²⁸ This consists in using the solution of the atom with the pseudopotential as a basis for the LCAO calculation; these pseudoatomic orbitals (PAO) are calculated with the boundary condition that they vanish outside a given radius r_c . The PAO's are, therefore, slightly excited, since their kinetic energy is increased due to the vanishing boundary condition.

They are strictly localized, which is very advantageous from the computational point of view. For a review of the quality of these PAO bases for electronic structure calculations, we refer the reader to Ref. 29. In this paper, we have used a radial cutoff of $r_c = 4.1$ Bohr.

The use of atomic orbitals, and a combination of efficient techniques, allow us to calculate the LDA Hamiltonian with an order- N effort (i.e., a cost that scales linearly with the number of atoms, both in time and in memory).²⁵ This makes it possible to reach system sizes with a much larger number of atoms than the standard techniques. Some of the Hamiltonian matrix elements are computed by interpolation of pre-calculated two- and three-center integral tables, whereas others are obtained by direct integration in a real-space grid. The fineness of the grid is expressed by the maximum kinetic energy of a plane wave that can be represented in it, as is usually done in plane wave calculations. Note that, in our case, the grid is used to represent the charge density, and not the wave functions. In this paper we have used a cutoff of 60 Ry for the grid integrations.

The solution of the Hamiltonian matrix can be done by straight diagonalization [which is an $\mathcal{O}(N^3)$ operation], or using recently developed order- N techniques,^{30,31} which are very advantageous for systems with large numbers of atoms (typically, the crossover between the two solutions is around 100 atoms, for calculations with minimal bases). The systems under study in this paper are in the range between 80 and 200 atoms, and therefore diagonalization of the Hamiltonian is feasible and competitive with an order- N technique. We have used diagonalization throughout this paper.

Calculations were performed for the following tubes: (4,4), (6,6), (8,8), (10,10), (10,0), and (8,4). They were all considered as isolated, infinitely long tubes. For that purpose, we used periodic-boundary conditions on a supercell geometry with sufficient lateral separation among neighboring tubes. For the purpose of sampling the Brillouin zone in the direction of the tube axis, as well as for the computation of the force-constant matrix for phonon calculations (see below), we used supercells containing several unit cells in the axis direction. The supercells consisted of five unit cells for the armchair (n,n) tubes [80, 120, 160, and 200 atoms for the (4,4), (6,6), (8,8), and (10,10) tubes, respectively], three unit cells for the zigzag (10,0) tube (120 atoms), and one unit cell for the chiral (8,4) tube (112 atoms). The supercell length in the tube-axis direction is similar for all of them, the number of atoms changing because of the different tube radii. Only the Γ point of the supercell was used in the phonon calculations, although more complete k -point samplings were tested showing no significant differences with the Γ -point results.

The atomic structures of the tubes were obtained by careful minimization of the total energy by means of the calculated Hellman-Feynman forces, including Pulay-like corrections to account for the fact that the basis set is not complete and moves with the atoms.²⁵ The minimizations were performed using a dissipative molecular-dynamics algorithm, which allows the geometry optimization with no symmetry conditions imposed. The residual forces in the optimizations were always smaller than 0.04 eV/\AA . The energy was minimized and the structure relaxed for different values of the lattice constant along the tube axis. This procedure allows us

to determine the most stable lattice constant along the tube, as well as the Young modulus and the Poisson ratio.

For the phonon calculations, we first obtain the force-constant matrix in real space using a finite-difference approach.^{32,33} We used finite-atomic displacements of 0.02 Å, and the force constants were taken as the average of the results obtained with positive and negative displacements, to eliminate anharmonic effects. All atoms are equivalent by symmetry, in the nanotubes, and therefore we only calculated the force constants for one of the atoms in the supercell, and generated the rest of the matrix using the symmetry operations.

The force-constant matrix has to be computed between a given atom and all the rest in the system. However, it is known that the force constants decrease rapidly with distance (in nonpolar systems), so that only the elements of atoms sufficiently close need to be computed. To do so, we set up a supercell large enough that a sufficient number of neighbors in the tube-axis direction is included. It must be also kept in mind that, in the supercell geometry, a given atomic displacement in the central cell is always accompanied by the same displacement of all the images. The supercell must, therefore, be large enough so that the effect of the image displacement is negligible. The cells discussed above were built with these observations in mind. Once the force-constant matrix in real space has been obtained, we calculate the dynamical matrix in reciprocal space, and diagonalize it to obtain the phonon modes and frequencies as a function of the one-dimensional (1D) crystalline momentum vector in the direction of the tube.

III. RESULTS AND DISCUSSION

A. Structural properties

We first study the equilibrium structural properties of the nanotubes. As a reference, we have first computed the equilibrium bond distance for a single-graphene plane, for which we obtain a value of $d=1.436$ Å, close to the experimental³⁴ (1.419 Å) and LDA plane-wave calculations³⁵ (1.415 Å) in graphite. Our value is slightly larger than the one obtained with plane waves, the small difference being due to the basis set. For all the tubes studied here we have found that the average carbon bond length is within 1% of the graphitic value. No appreciable symmetry-breaking distortions have been observed. However, by symmetry, for the (n,n) and $(n,0)$ tubes there are two inequivalent bonds, three in general, for chiral tubes. Figure 1(a) shows the value of these two bond lengths as a function of tube radius (in units of the graphene bond length) for the (n,n) tubes studied here. The differences between these bonds and graphite, and between the two kinds of bonds, are small but significant. Two effects are apparent: (i) both bond lengths increase (as compared with the graphene reference) with decreasing tube radius; (ii) the difference between them also increases with decreasing radius. Both effects can be easily understood in terms of the rehybridization and the weakening of the π bonds induced by the curvature.⁶ As shown in Fig. 1(a), the longer bond is the one perpendicular to the tube axis in the (n,n) tubes. This is in contrast with the results of Ref. 7. This discrepancy is due to the small k -point sampling used in that paper.³⁶

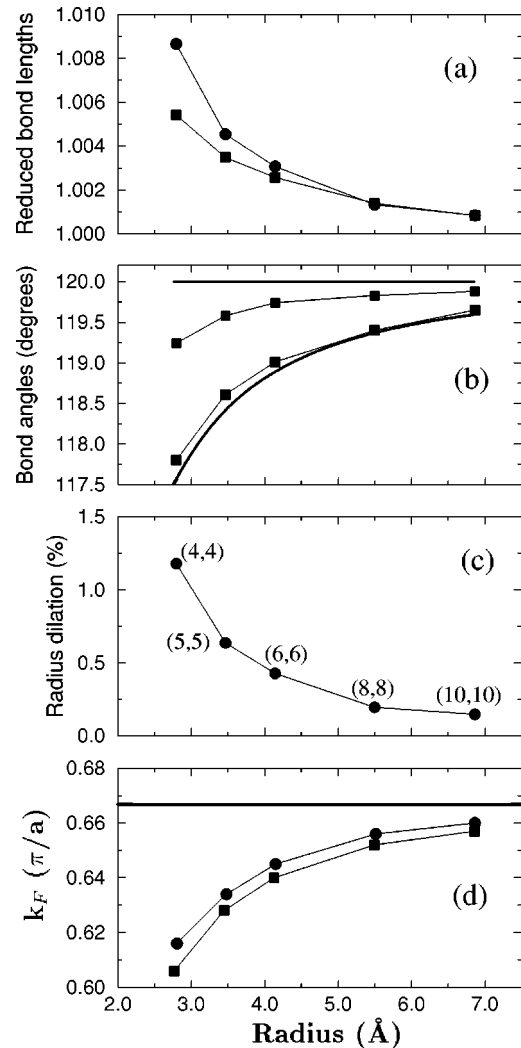


FIG. 1. Structural and electronic variations with tube radius. (a) Length of the two inequivalent bonds in (n,n) tubes in units of the bond length in graphite. Circles are for the bond perpendicular to the tube axis, and the squares for the other inequivalent bond length. (b) The two inequivalent bond angles in (n,n) tubes. Continuous lines show the angles resulting from an ideal graphene rolling. (c) Tube-radius dilation as compared to the ideal radius. (d) Position of the Fermi surface (k_F) in the Brillouin zone. Squares and circles stand for the ideal and relaxed structures, respectively. The continuous line indicates the ideal zone-folded value.

Figure 1(b) shows the variation of the bond angles with the tube radius for the (n,n) tubes. As for the bond distances, there are two inequivalent bond angles in (n,n) tubes. The behavior of the bond angles is very similar to the one expected from ideal “rolling” of a graphene plane to form the tube, also shown in Fig. 1(b). In this case, one of the angles would maintain a value of 120° , whereas the other would decrease for smaller tube radii, leading to the increasing tube curvature. In the fully relaxed structures, both angles are smaller than 120° , so that the curvature stress is more distributed around the tube area. Since the ideal 120° angle now shares some of the cost of the curvature, the other angle increases slightly from its ideal value. Nevertheless, we see that deviation from the ideal behavior is only relevant for the tubes with small radius, being almost negligible for tubes larger than (6,6).

As a consequence of the increase in bonding distances shown in Fig. 1(a), the actual tube radii are slightly larger than those resulting from an ideal rolling of the graphene sheet. This is plotted in Fig. 1(c). Again, this deviation is more pronounced for the tubes with smaller radius, and the behavior approaches the ideal for large radii tubes.

The structural distortions affect the electronic structure of these metallic tubes. Although the study of the electronic properties is not the focus of this paper, it is worth discussing what is the effect of the structural parameters on the Fermi level, since this has implications for the physics of these systems, for example, in the interpretation of very recent scanning tunneling spectroscopy experiments on short SWNT.³⁷ In a zone-folding model based on the graphene band structure, the Fermi level of all (n,n) tubes would be located at a wave vector of $\frac{2}{3}\pi/L$ (with L being the lattice constant in the tube axis). For the real tube structure, the position of the Fermi level will change due to the reduced symmetry, with its two inequivalent bonds (those perpendicular to the tube axis, and those nonperpendicular). In a simple Hückel model this reduced symmetry is described with two different hopping interactions t_{\perp} and t' , both different from the ideal graphene hopping t . The Fermi wave vector in this case is $k_F = (2/L)\arccos(t_{\perp}/2t')$. In real tubes, the Fermi surface moves because of two reasons: (i) The rolling of the graphene plane to form the tube originates a change of the electronic potential in the inequivalent bonds of the tube, even in the case where the structure is taken as the ideal graphene rolling, i.e., with both bonds kept at the same graphene bond length. (ii) The difference in bond lengths for the two inequivalent bonds in the relaxed structure change the hopping matrix elements. In order to distinguish these two effects, we show in Fig. 1(d) the calculated values of the Fermi wave vector for the fully relaxed structures, and for the ideal graphene rolling tubes, obtained with our LDA-LCAO formulation. We see that the main effect of the Fermi level shift is the rolling to form the tube, whereas the difference in bond lengths brought by the structure relaxation gives only a minor correction tending to bring k_F closer to the graphene value. We see that the deviation from the graphene Fermi level are relatively large, increasing with decreasing tube radii.

B. Elastic properties

1. Strain energy

Figure 2(a) shows the strain energy per atom (energy relative to a planar graphene sheet) as a function of the radius of the tube. The data follows quite well the behavior expected from classical elasticity theory,³⁸ $E_{st} = C/r^2$, where r is the radius of the tube and C is a constant that depends on the Young modulus Y and thickness h of the wall in a model tube: $C = Yh^3a/24$. A least-squares fit to the results of the (n,n) tubes yields a value of $C = 2.00 \text{ eV \AA}^2/\text{atom}$, in very good agreement with recent LDA calculations.⁷ For the other two tubes studied, (8,4) and (10,0), we obtain slightly larger values (2.15 and 2.16 $\text{eV \AA}^2/\text{atom}$, respectively).

It is to some extent surprising that the predictions from elasticity theory are so closely followed by the detailed *ab initio* calculations. In fact, the assignment of a thickness h for a single atomic layer is not a well-defined procedure.

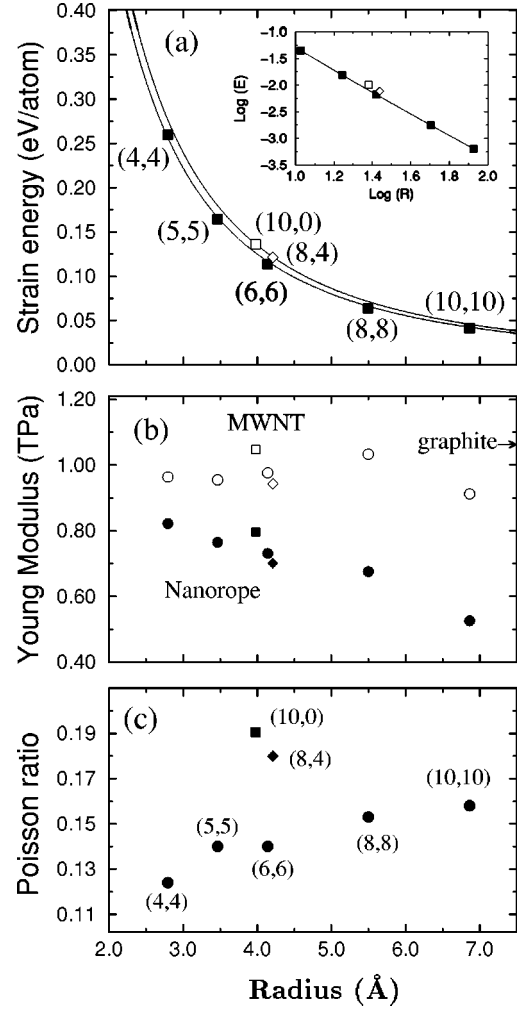


FIG. 2. (a) Strain energy versus tube radius. Solid line drawn across the (n,n) data corresponds to a least-squares fit to the C/r^2 behavior. The two C/r^2 functions passing through the (8,4) and (10,0) data are also shown (in this scale they appear as one line). The $r^{-\alpha}$ behavior is clearly shown in the inset. The value obtained for α from the logarithmic fit is 2.05 ± 0.02 . (b) Young modulus versus tube radius. Open symbols for the *multiwall* geometry, and solid symbols for the *single-wall-nanotube* crystalline-rope configuration. The experimental value of the c_{11} elastic constant of graphite is also shown. (c) Poisson ratio versus tube radius.

Adams *et al.*³⁹ provided an alternative explanation based on microscopic arguments. They use a very simplified model in which the energetics of many different fullerene structures depend on a single structural parameter: the *planarity* ϕ_{π} , which is the angle formed by the π orbitals of neighbor atoms. Assuming that the change in total energy is mainly due to the change in the t_{π} interaction between these orbitals, and that this change is proportional to $\cos \phi_{\pi}$, the r^{-2} behavior is predicted. Adams *et al.* obtained a value of $C = 2.12 \text{ eV \AA}^2/\text{atom}$ using non-self-consistent first-principles calculations. Previous calculations using Tersoff and Tersoff-Brenner potentials¹³ predict the same dependence and gave a value of $C \approx 1.5$ and $1.2 \text{ eV \AA}^2/\text{atom}$, respectively.

We note in Fig. 2(a) that the (n,n) tubes are energetically more stable as compared to other chiralities with the same radius. This difference is, however, very small and will de-

crease as the tube diameter increases due to the r^{-2} behavior. This is expected, since in the limit of large radii the same graphene limit is obtained, regardless of chirality.

2. Young modulus

Measurements of the amplitude of the intrinsic thermal vibrations of the tubes¹¹ allow an indirect determination of the Young modulus, yielding an average value of 1.8 TPa. There is a large uncertainty in the results, however, with values ranging from 0.40 to 4.15 TPa. Furthermore, measurements of the restoring force on bent nanotubes with an atomic-force microscope give an average value of 1.28 ± 0.59 TPa. Since the corresponding elastic constant for graphite (c_{11}) is also of the order of 1 TPa, it is still a question whether the rolling of the graphene plane to obtain nanotubes increases or decreases its stiffness.

Theoretical calculations can help in solving the issue, but the calculations performed so far also show a great dispersion in their predictions. Some theoretical estimates report values of the order of 5 TPa (Ref. 40) based on an empirical Keating force-constant model for the finite-capped (5,5) tube. This unreasonably high value can be due to the small size of the aggregates used to describe the tube, with only up to 400 atoms. Yakobson *et al.*,⁹ in a study of the structural instabilities of SWNT for large deformations, and using Tersoff-Brenner potentials, obtain an estimate for the Young modulus of about 5.5 TPa, by fitting their results to the continuum elasticity theory. However, Robertson *et al.*,¹³ using the same potential, report a small weakening of the stiffness of nanotubes as the diameter decreases, and therefore a Young modulus for the nanotubes smaller than the one of graphene. They find a systematic dependence with the chirality which, although being small, increases with decreasing tube radius. Lu,¹⁵ using a force-constant model fitted to reproduce the phonons and elastic constants of graphite, obtains elastic properties that are essentially independent of helicity and tube radius, and comparable to those of graphene (with values of the Young modulus below 1 TPa). Finally, recent tight-binding¹⁶ calculations give values of the order of 1 TPa for the SWNT, quite insensitive to the chirality of the nanotube, and mainly determined by the tubule diameter, approaching the graphitic limit for diameters of ~ 1.2 nm.

Part of the discrepancies in the theoretical results discussed above is merely due to a different definition of the Young modulus in these systems. From the point of view of elasticity theory, the definition of the Young modulus involves the specification of the value of the *thickness* of the tube wall. As discussed in the previous section, it is not clear how to define this width for a SWNT, where the wall is composed of only one shell of atoms. The anomalously large value obtained by Yakobson *et al.*⁹ is due to an assignment of a value of $h=0.6$ Å for the thickness of the graphene plane, which is obviously too small. Other authors^{15,16} have used the graphite interlayer spacing of 3.4 Å in their calculations.

In order to avoid this definition problem, we have analyzed our results on the elastic stiffness of the nanotubes using the second derivative of the strain energy with respect to the axial strain: $d^2E/d\epsilon^2$. To obtain this quantity for the different tubes, we have performed structural relaxations for the nanotubes, subject to deformations between -1.0% and

TABLE I. Calculated values of $d^2E/d^2\epsilon$ for different tubes. The values for a graphene plane obtained with different supercells are also shown (see text for details).

Tube	R (Å)	$d^2E/d^2\epsilon$ (eV)
(4,4)	2.794	56
(5,5)	3.463	55
(6,6)	4.140	56
(8,8)	5.498	59
(10,10)	6.864	52
(8,4)	4.211	54
(10,0)	3.979	60
Graphene (4,4)		50
Graphene (10,10)		54
Graphene (large)		60

1.0%, at intervals of 0.13%. The total energies for deformations in the interval $(-0.75\%, 0.75\%)$ were fitted to a third-order polynomial, and $d^2E/d\epsilon^2$ was obtained from the second derivative at zero strain. The results are shown in Table I. We have estimated the numerical error of these results by taking different intervals in the fitting procedure: $(-0.5\%, 0.5\%)$ and $(-1.0\%, 1.0\%)$, and obtain that the typical uncertainty of the calculation of $d^2E/d\epsilon^2$ is of the order of 10%. From Table I we see that the average value in the tubes is about 56 eV. The variation between tubes with different radii and chirality is very small, and always within the limit of accuracy of the calculation. We therefore can conclude that the effect of curvature and chirality on the elastic properties is small.

For comparison, we have also calculated the values of $d^2E/d\epsilon^2$ for a single graphene sheet. Three calculations were done, with different supercells. In all the cases, only the Γ point of the supercells was used reproducing the k -point sampling of the tube calculations. Two of them were the unrolled equivalents of the supercells used for the (4,4) and (10,10) tubes. These cells were used to allow for a direct check of the curvature effects, comparing the planar and tubular geometry. The third one was a rectangular (nearly square) cell of 17.41×17.23 Å, with 112 atoms, thus providing a more uniform k -point sampling, and, therefore, a more confident estimation of the elastic constant. The results (also displayed in Table I) clearly show that there are no appreciable differences between the results obtained for the nanotubes and those of graphene, the differences being within the uncertainty of the calculation. These data confirm that the effect of curvature on the Young modulus of the SWNT is small down to radii of the order of, at least, 2.8 Å.

Our results are in good agreement with those obtained by Robertson *et al.*¹³ using Tersoff-Brenner potentials, who find values around 59 eV/atom, with very little dependence with radius and/or chirality. Furthermore, we can obtain an experimental estimate of this quantity using the elastic constant¹³ $c_{11}=1.06$ TPa of bulk graphite, from which we obtain $d^2E/d\epsilon^2 \approx c_{11}V_a = 58.2$ eV/atom (where V_a is the atomic volumen in graphite). This value agrees well with the results obtained here, and with those of Robertson *et al.*¹³

If one insists on calculating the Young modulus using the standard bulk definition, instead of the well-defined second derivative used above, one must choose a definition of the

effective area per carbon atom. Here we calculate the Young moduli considering two different geometries: (i) a *multiwall-like* geometry, in which the normal area is calculated using the wall-wall distance as the one in multiwall tubes, which is very approximately equal to the one of graphite, i.e., the effective *thickness* of the tube wall is taken to be 3.4 \AA , and (ii) a rope configuration of single wall tubes, where the tubes would be arranged forming a hexagonal closed packed lattice, with a lattice constant of $(2r + 3.4 \text{ \AA})$, being r the tube radius. The results are shown in Fig. 2(b). For the crystalline rope geometry, the decrease of the Young modulus with increasing the tube radius is due to the quadratic increase of the effective area in this configuration, while the number of atoms increases only linearly with the tube diameter. The computed values for the SWNT ropes are, however, still very high, even comparing with other carbon fibers.⁴¹

3. Poisson ratio

The Poisson ratio ν is given by the variation of the radius of the SWNT resulting from longitudinal deformations along the tube axis:

$$\frac{\Delta r}{r} = -\nu \frac{\Delta l}{l} \quad (1)$$

where l is the tube length. We have calculated ν for the tubes under study, and find that in all cases the Poisson ratio is positive: an elongation of the tube reduces its diameter. The results are shown in Fig. 2(c). We obtain values around $\nu = 0.14$ (from 0.12 to 0.16) for the armchair (n,n) tubes, and a little larger for other chiralities: 0.19 for (10,0) and 0.18 for (8,4). The uncertainty of the obtained values is of the order of 10%. These results reveal a slight decrease of the Poisson ratio with the tube radius, and a stronger dependence with chirality. Our results are close to the value of $\nu=0.19$ obtained by Yakobson *et al.*⁹ using Tersoff-Brenner potentials, but considerably smaller than the value $\nu=0.28$ given by Lu¹⁵ with a force-constant model and $\nu=0.26$ from a tight-binding calculation.¹⁶ The corresponding magnitude along the basal plane in graphite is $\nu=0.16$.^{42,43}

C. Vibrations

In our study of the vibrational properties of SWNT, we have first computed the phonon spectrum of a single graphene plane, which is shown in Fig. 3(a). This will serve as a test of the accuracy of the calculation method, and as a reference for the interpretation of the nanotube results. Also, the graphene-phonon structure is needed to obtain nanotube phonons within the zone-folding approach.

The calculation of the graphene phonons has been performed using the nearly square supercell of 112 atoms described in previous sections. The calculated *ab initio* phonon-dispersion curves are, in general, in quite good agreement with experiments for graphite.⁴⁴ The most remarkable disagreement is for the frequency of the higher-optical bands, which at Γ is around 1690 cm^{-1} in our calculations, and 1580 cm^{-1} in the experiment. This difference is attributed to the use of a minimal sp^3 basis in the calculation. However, our calculations reproduce well the overbending of the LO band (i.e., the highest frequency is not at the Γ point, but at intermediate points between ΓM and ΓK).

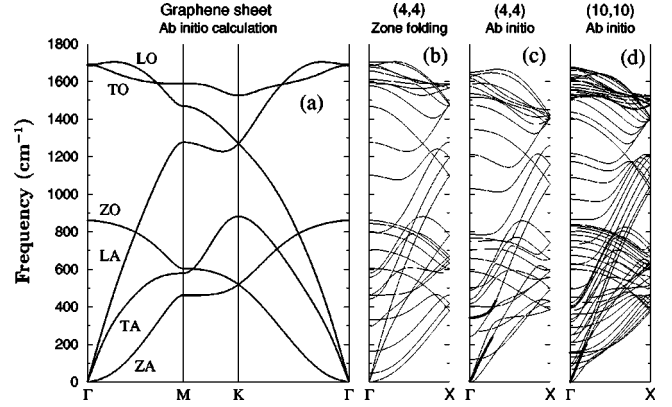


FIG. 3. (a) Calculated phonon structure for a graphene sheet. (b) Zone-folding result for the (4,4) tube, obtained from the graphene *ab initio* phonons in panel (a). *Ab initio* dispersion relations for the (4,4) (c), and the (10,10) (d) nanotubes. In (c) and (d), thicker lines are used to mark two special branches: the acoustic band is a twiston mode (torsional shape vibrations), the other (with finite frequency at Γ) is the breathing mode.

This has important consequences in the phonon structure of the nanotubes, especially in the zone-folding scheme, where the overbending leads to Raman-active modes in the nanotubes, which are higher in frequency than those of graphene. Also, our results show good quantitative agreement with experiment for the lower-frequency band. For example, for the out-of-plane (Z direction of graphene) transversal-optical mode [labeled in Fig. 3(a) as (ZO)], we obtain a frequency of 861 cm^{-1} , to be compared with the corresponding infrared-active mode in bulk graphite of 868 cm^{-1} . Acoustic bands are also well reproduced.

The main features in the phonon dispersion of Fig. 3(a) are in good agreement with other density-functional calculations,^{45,46} but differ from the phonon bands obtained with empirical force-constant models,^{23,47} especially around the M point.

Sound velocities are extracted from the slope of the acoustic branches. We obtain 24 km/s and 18 km/s for the LA and the in-plane TA branches, respectively. These results agree very well with the sound velocities that can be extracted from the experimental data of Ref. 44 for the graphite (0001) surface phonons, ≈ 24 and 14 km/s . The out-of-plane transversal band [(ZA) in Fig. 3(a)] has a zero sound velocity. Fitting the frequencies below 80 cm^{-1} to a parabolic function $\omega = \delta q^2$, a value of $\delta \approx 6 \times 10^{-7} \text{ m}^2 \text{ s}^{-1}$ is obtained, in very good agreement with previous estimations.⁴⁹

The sound velocities of the LA and TA branches allow us to calculate back the in-plane stiffness (71.6 eV/atom) and the shear modulus (40.3 eV/atom) of the graphene sheet, respectively. Both values are higher than the ones obtained directly (see previous subsection) due to error propagation: the elastic constants depend quadratically on the sound velocities, and these are delicate to obtain due to numerical problems close to the Γ point. The other way around, the sound velocity calculated using the experimental basal-plane shear modulus of bulk graphite ($c_{66}=0.44 \text{ TPa}$ ⁴²) is 14 km/s , which is indeed quite close to our value.

From the quadratic behavior of the ZA band we can also estimate the energy necessary to roll up the graphene plane to form the tubes. It can be easily shown that the strain

energy per carbon atom can be approximated by $E_{st} = C/r^2$ where $C = \delta^2 m_c / 2$, being m_c the carbon atom mass and r the tube radius. The value obtained for C is $2.3 \text{ eV \AA}^2/\text{atom}$, which is only 7% higher than the calculated constant for the (10,0) and (8,4) tubes, and 13% higher than the same constant for (n,n) tubes.

We next investigate the phonon structures of the nanotubes considered here. Let us first comment on the numerical errors in the calculated vibrational frequencies. These are mainly originated from the residual forces in the structural relaxation, the finite atomic displacements in the force-constant matrix calculation, and the finite grid utilized in the integration of the Hamiltonian matrix elements. We have estimated this numerical error from the differences in the frequencies obtained for the (10,0) tube by displacing two different (but equivalent by symmetry) atoms for the calculation of the force-constant matrix. We find that the error is about 10 cm^{-1} for the high part of the spectrum (frequencies higher than 1300 cm^{-1}), and could increase up to 30 cm^{-1} for some of the lower branches. The breathing mode and the acoustic bands are more stable, showing errors of about 15 cm^{-1} . Uncertainties of the same magnitude have been reported by other authors performing similar calculations on graphitic systems.^{46,48}

Figures 3(c) and 3(d) show the calculated *ab initio* 1D dispersion relations for the armchair (4,4) and (10,10) tubes. The zone-folding results for the tube (4,4), obtained from the graphene *ab initio* dispersion relations, are also displayed in the panel (b) of the same figure. The difference between the *ab initio* and the zone-folding frequencies are a consequence of curvature and relaxation effects, and are, therefore, a measure of their importance in the phonon spectrum.

From the results of Fig. 3 we see that, apart from some small differences, which we will analyze in the following, the general agreement between the *ab initio* results and the zone-folding predictions is considerably good. This is the case even for the tubes with smaller radii, where the curvature effects in the phonon frequencies are expected to be more important, and the zone-folding scheme could start to break down. The agreement is particularly good for the upper part of the spectrum, and worsens for decreasing frequencies. This is mainly due to the failure of the zone-folding approach to describe the breathing modes and two of the acoustic bands of the tube (those corresponding to motion in the directions perpendicular to the tube axis). In particular, within the zone-folding scheme, the breathing mode appears with zero frequency, and the two translational modes appear with finite frequency. It should be noticed that these deficiencies can be corrected,²³ and an analytical expression can be obtained for the breathing mode frequencies making similar assumptions as those made in the zone-folding scheme: the use of force constants from a graphene plane. Jishi *et al.*²³ showed that this model predicts a $1/r$ dependence of the frequency of this mode, regardless of chirality.

The deficiencies mentioned above are absent in the *ab initio* results, without having to resort to additional corrections. In Figs. 3(c) and 3(d) we display with thicker lines the phonon bands associated with the breathing and twiston modes for the *ab initio* results.

The twistons are torsional acoustic modes, which have been proposed to be of relevance for the peculiar linear de-

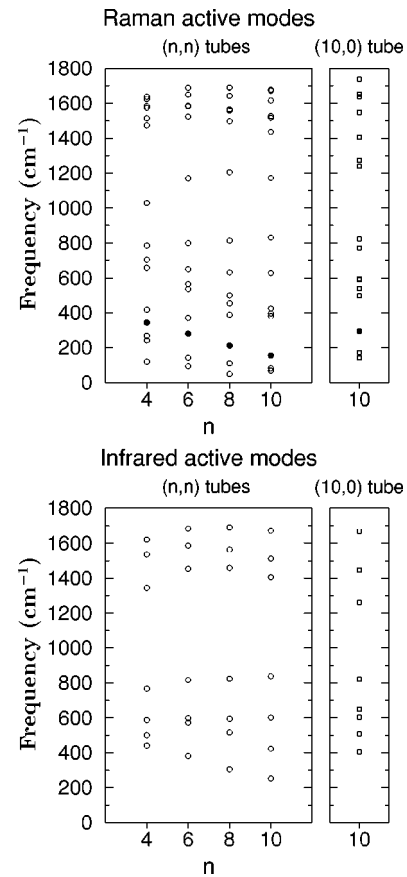


FIG. 4. *Ab initio* frequencies of the Raman and infrared active modes for the (n,n) series and for the (10,0) nanotube. Filled symbols indicate the breathing mode.

pendence of the electrical resistivity with temperature in the metallic (n,n) tubes.⁴ These vibrational modes break the reflection symmetry of the tubes, and open a gap at the Fermi level, producing a strong electron-phonon coupling, key to the understanding of that behavior. The sound velocity of these modes is, therefore, important for the electronic properties of the (n,n) tubes. Our results indicate that the twiston mode sound velocity is lower than the corresponding value obtained for graphene (TA band) for all the studied tubes, and slowly diminish with decreasing tube radius. For the (10,10) tube, the twiston sound velocity is 15 km/s , i.e., 17% lower than the value found in the graphene plane, and for the narrower tube (4,4) the value decreases to 13 km/s .

Figure 4 shows the Raman and infrared active modes at the Γ point. These have been assigned according to the D_{nd} groups,²³ which predict 7 infrared-active modes and 15 Raman-active modes for the (n,n) tubes, and 8 infrared- and 16 Raman-active modes for the $(n,0)$ regardless of their radius. We note that, for the (10,0) tube, the highest Raman-active mode in the *ab initio* calculation has a frequency larger than the corresponding frequencies for the (n,n) tubes. In our calculation this highest Raman active mode has a frequency even larger than that predicted by the zone-folding scheme. This is in contrast with the findings for the (n,n) tubes. In the (10,0) tube, this mode corresponds to an optical vibration in which the displacement vector is parallel to the tube axis. Although the position of this mode is quite sensitive to the numerical precision of the calculation (and in

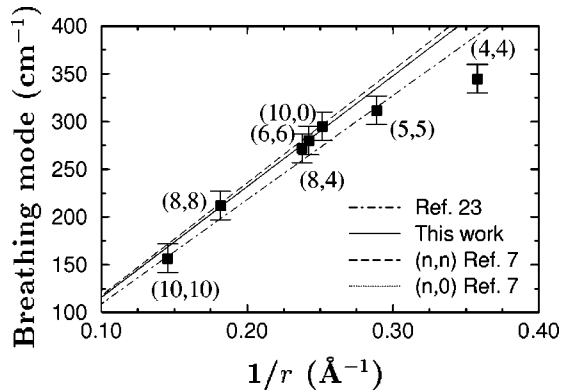


FIG. 5. *Ab initio* breathing mode frequencies as a function of the inverse tube radius, for (8,4), (10,0) and five (n,n) tubes. The continuous line is a linear fit to the data excluding the (4,4) and (5,5) tubes. Dot-dashed line shows the behavior obtained by Jishi *et al.* (Ref. 23) using a force-constants model. Dashed and dotted lines show the result of the LDA calculations by Kürti *et al.* (Ref. 7) for the (n,n) and $(n,0)$ tubes, respectively. In this scale the dotted line is hidden by the continuous one. Error bars as estimated (see the text).

particular to the Brillouin zone sampling utilized), we can conclude that this tube presents optical frequencies that are higher than those of (n,n) tubes with comparable radii.

We have also analyzed the dependence of the breathing mode frequency with the tube radius and chirality. The results are shown in Fig. 5. The breathing mode is a A_{1g} symmetry mode (being, therefore, Raman active), in which there is a monopolar inward and outward vibration of the atoms. A simple approach, based on the force constants derived from the graphene plane, predicts a change of the frequency of this mode as A/r , independently of chirality, where r is the tube radius and $A = 1092 \text{ cm}^{-1} \text{ \AA}$.²³ Recent LDA frozen-phonon calculations⁷ of this mode confirm the prediction of the r^{-1} behavior, the constant A having a weak dependence on chirality, 1180 and $1160 \text{ cm}^{-1} \text{ \AA}$ for (n,n) and $(n,0)$, respectively. Our calculations confirm the previous results, indicating once again that the effect of curvature on the value of the force constants is small, even for the small radii tubes considered here. Only the (4,4) tube presents an important deviation from the predicted behavior, with an appreciable decrease in the breathing-mode frequency. This effect is already noticeable in the (5,5) tube, although to a smaller extent. This effect can be understood as a consequence of the hybridization changes and the decrease of the π interaction, induced by the curvature. A r^{-1} fit of the results for tubes with radius greater than 3.8 \AA gives a value of $1160 \text{ cm}^{-1} \text{ \AA}$ for the constant A , in very good agreement with Ref. 7, as clearly shown in Fig. 5. The possible chirality dependence of the breathing mode, if any, is well below the resolution of our data. As pointed out in Ref. 7, the value of A can be estimated from the stretching constant of the graphene plane neglecting all the possible effects of curvature. Taking our calculated value of 60 eV/atom (see previous sections) for this elastic constant, we obtain a value $A = 1166 \text{ cm}^{-1} \text{ \AA}$.

One of the most important differences between the *ab initio* and zone-folding frequencies is a general softening of frequencies when curvature effects are taken into account. This is especially clear for the higher-frequency bands, but is

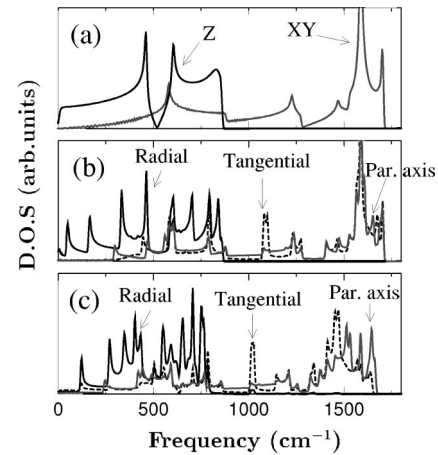


FIG. 6. Vibrational density of states for (a) graphene, (b) the (4,4) tube in the zone-folding approximation, and (c) the *ab initio* results for the same tube. The curves are decomposed in the different directions of the displacement vector. For graphene, Z indicates modes perpendicular to the plane, and X and Y within the plane. For the (4,4) tube, the modes are decomposed in radial, tangential, and parallel to the tube axis.

also observable for the intermediate frequencies. The shift is not uniform, and therefore the distribution and, in some cases, the ordering of the Raman- and Ir-active modes are affected by curvature effects. This effect is most evident in the (4,4) tube, where the curvature is more pronounced. We show in Fig. 6 the vibrational density of states for the (4,4) tube, comparing the *ab initio* and the zone-folding results. The figure shows the decomposition of the modes in radial and tangential (parallel and perpendicular to the tube axis). We see that the radial modes correspond to frequencies below 800 cm^{-1} , corresponding roughly to the out-of-plane bands of graphene. The softening of the frequencies in the *ab initio* calculation are apparent in this figure, especially for the higher-frequency modes. Also, the upper limit of radial vibrations is lowered by about 100 cm^{-1} in the *ab initio* calculation compared with the zone-folding results, for the (4,4) tube.

Several papers^{17,19} have recently made use of the frequency of the higher optically active modes as an experimental signature of the tube radii. In graphite there is only one Raman-active optical mode (with zero wave vector) at 1580 cm^{-1} , which in our calculation appears at 1690 cm^{-1} . In the nanotubes, it splits into multiple peaks, which are originated in the zone folding of the graphene bands. The frequencies of these $q_z=0$ tube modes depend on radius and chirality. In the zone-folding scheme, these modes sample the corresponding optical bands of graphite, with wave vectors $q_n = n/r$ ($n=0,1,2, \dots$) along the circumference direction. Of these, only a small number (independent of the tube radius) are Raman or Ir active.^{23,47} Kasuya *et al.*¹⁹ were able to measure the frequency of the highest Raman modes for tubules with different radii, and found that these corresponded to the $n=1$ LO band, and $n=1$ and $n=2$ TO bands of graphite (in order of decreasing frequencies). They found the value of the observed frequencies to be in excellent agreement with the direct zone-folding results. The radius of the narrower tubes in their sample was 5.5 \AA , which, assuming an armchair conformation, would correspond to the (8,8) tubule. It is, therefore, interesting to see whether these results are modi-

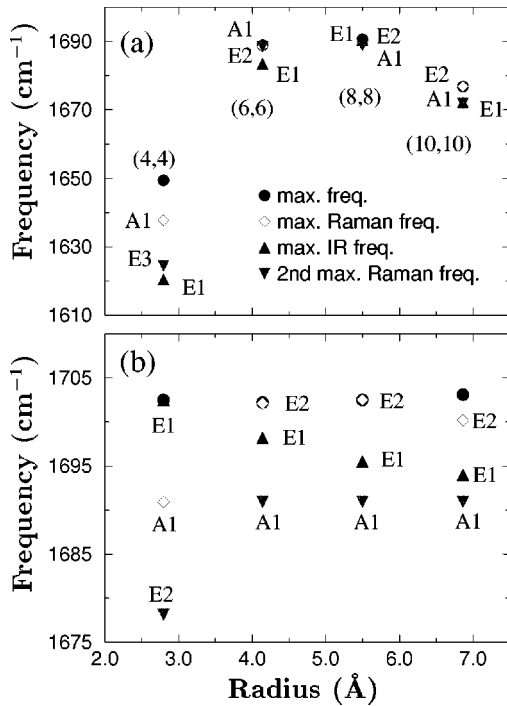


FIG. 7. Frequencies for the higher optical modes for different tubes, (a) *ab initio*, and (b) from the zone-folding scheme. We show the frequencies of the highest vibrational mode, the two highest Raman-active modes, and the highest Ir-active mode. The symmetry of each mode is also shown.

fied for tubes with smaller radii, as was the case for the breathing mode discussed above.

Figure 7(a) shows the frequencies of the higher-optical modes obtained from the *ab initio* calculation, whereas Fig. 7(b) shows the results from the zone-folding approach. Several facts are worth noticing in the comparison. As was the case for the breathing mode, the (4,4) tube deviates very significantly from the zone-folding behavior. The maximum *ab initio* frequency is about 50 cm^{-1} lower than the zone-folding prediction, and the symmetries and activities of the higher-frequency peaks are very different. For the larger tubes, it seems that the *ab initio* results tend to confirm the symmetry assignments of the zone-folding approach, supporting the analysis of experimental results in terms of the simple zone-folding scheme. The apparent softening of the maximum frequencies for the (10,10) tube in Fig. 7(a) is due to numerical error (the 10 cm^{-1} error bar discussed above, possibly slightly larger for the largest tube). The maximum frequency for this tube should approach the one obtained by the zone-folding method since the curvature is the smallest. This serves as a measure of the accuracy of our calculation.

IV. CONCLUSIONS

We have presented the results of *ab initio* calculations for single-wall carbon nanotubes with different chiralities and radii, addressing structural, elastic, and vibrational properties. The cases studied include (n,n) tubes (with n ranging from 4 to 10), and the (8,4), and (10,0) tubes. We have also presented a detailed comparison with the results of other usual approaches like elasticity theory for elastic properties

or the zone-folding approach for the vibrations. Our results serve to validate most of the predictions of these simpler theories, and to point out their limits of applicability. The following conclusions can be drawn from our results:

(i) Relaxation effects due to the tube curvature are small in general. The inequivalent bonds in a tube enhance their differences in bond length and angles with decreasing tube radius. The symmetry inequivalent bonds give rise to a small shift in the Fermi surface location for the (n,n) tubes, mainly related to the lower symmetry of the tubes as compared with graphene, and only slightly modified by the structural relaxation.

(ii) The strain energy follows the α/r^2 law expected from elasticity theory quite accurately for tubes as narrow as (4,4). For armchair tubes, which have slightly lower strain energy than other chiralities, the constant has a value of $\alpha = 2.00 \text{ eV\AA}^2/\text{atom}$.

(iii) Sensible definitions of the Young modulus are used for two different geometries: multiwall and single-wall tubes. In the former case the values are very similar to the one of graphite. Single-wall tubes show values smaller than graphite. In any case, we propose the elastic constant per unit mass as the relevant quantity, since it does not depend on the geometry of the system. This is shown to be quite similar to the correspondent quantity in graphite, for all the studied tubes, and larger than in any known fiber.

(iv) The Poisson ratio also retains graphitic values except for a possible slight reduction for small radii. It shows a chirality dependence: (n,n) tubes display smaller values than (10,0) and (8,4). Our results for the (n,n) tubes are consistent with the experimental basal Poisson ratio of graphite.

(v) The phonon bands behave as expected from simple schemes, except for slight deviations, which become more important for the narrower tubes. The zone-folding analysis gives a good qualitative (and sometimes quantitative) picture of many of the properties studied here, except for known deficiencies in the low-frequency vibrational spectra. For the smallest radii, the zone-folding description of the high-frequency vibrations is insufficient, too.

(vi) The breathing mode follows the A/r law predicted by graphene-derived force-constants calculations. The obtained value of A is consistent with that calculated from the in-plane stretching elastic constant of graphene. It, however, seems to soften with respect to the expectations for the smallest radii tubes, like (4,4). A similar softening is observed for the twiston modes, whose sound velocity diminishes for decreasing radii.

(vii) The high-frequency optic modes are sensitive to the kind of tube and to its radius. The frequencies of the highest modes tend to diminish with decreasing radii by effect of the curvature.

ACKNOWLEDGMENTS

We are grateful to Javier Junquera for giving us the possibility of performing k -sampling tests with his code. We acknowledge financial support from DGICYT under Grant No. PB95-0202, and from European Community TMR Contract No. ERBFMRX-CT96-0067 (DG12-MIHT).

- ¹*Nanotubes*, edited by S. Iijima and M. Endo, special issue of Carbon **33**, 869–1019 (1995); T. W. Ebbesen, Phys. Today **49**(X), 26 (1996); P. M. Ajayan and T. W. Ebbesen, Rep. Prog. Phys. **60**, 1025 (1997); A. Rubio, Condens. Matter News **6**, 6 (1997), and references therein.
- ²A. Thess, R. Lee, P. Nikolaev, H. Dai, P. Petit, J. Robert, C. Xu, Y. H. Lee, S. G. Kim, A. G. Rinzler, D. T. Colbert, G. E. Scuseria, D. Tomanek, J. E. Fisher, and R. E. Smalley, Science **273**, 483 (1996).
- ³C. Journet, W. K. Maser, P. Bernier, A. Loiseau, M. Lamy de la Chapelle, S. Lefrant, P. Deniard, R. Lee, and J. E. Fisher, Nature (London) **388**, 756 (1997).
- ⁴C. L. Kane and E. J. Mele, Phys. Rev. Lett. **78**, 1932 (1997); C. L. Kane *et al.*, Europhys. Lett. **41**, 683 (1998).
- ⁵Jae-Yel Yi and J. Bernholc, Phys. Rev. B **47**, 1708 (1993); J. W. Mintmire, D. H. Robertson, and C. T. White, J. Phys. Chem. Solids **54**, 1835 (1993); J. W. Mintmire and C. T. White, Carbon **33**, 893 (1995).
- ⁶X. Blase, L. X. Benedict, E. L. Shirley, and S. G. Louie, Phys. Rev. Lett. **72**, 1878 (1994); X. Blase, A. Rubio, S. G. Louie, and M. L. Cohen, Europhys. Lett. **28**, 335 (1994).
- ⁷J. Kürti, G. Kresse, and H. Kuzmany, Phys. Rev. B **58**, R8869 (1998).
- ⁸S. Iijima, C. Brabec, A. Maiti, and J. Bernholc, J. Chem. Phys. **104**, 2089 (1996).
- ⁹B. I. Yakobson, C. J. Brabec, and J. Bernholc, Phys. Rev. Lett. **76**, 2511 (1996); B. I. Yakobson and R. E. Smalley, Am. Sci. **85**, 324 (1997).
- ¹⁰M. R. Falvo, G. J. Clary, R. M. Taylor, II, V. Chi, F. P. Brooks, Jr., S. Washburn, and R. Superfine, Nature (London) **389**, 582 (1997).
- ¹¹M. M. J. Treacy, T. W. Ebbesen, and J. M. Gibson, Nature (London) **381**, 678 (1996).
- ¹²E. W. Wong, P. E. Sheedan, and C. M. Lieber, Science **277**, 1971 (1997).
- ¹³D. H. Robertson, D. W. Brenner, and J. W. Mintmire, Phys. Rev. B **45**, 12 592 (1992), and references therein.
- ¹⁴R. S. Ruoff and D. C. Lorents, Carbon **33**, 925 (1995); C. F. Cornwell and L. T. Wille, Solid State Commun. **101**, 555 (1997).
- ¹⁵J. P. Lu, Phys. Rev. Lett. **79**, 1297 (1997); J. Phys. Chem. Solids **58**, 1649 (1997).
- ¹⁶E. Hernández, C. Goze, P. Bernier, and A. Rubio, Phys. Rev. Lett. **80**, 4502 (1998).
- ¹⁷A. M. Rao, E. Ritcher, S. Bandow, B. Chase, P. C. Eklund, K. A. Williams, S. Fang, K. R. Subbaswamy, M. Menon, A. Thess, R. Smalley, G. Dresselhaus, and M. S. Dresselhaus, Science **275**, 187 (1997).
- ¹⁸E. Richter and K. R. Subbaswamy, Phys. Rev. Lett. **79**, 2738 (1997).
- ¹⁹A. Kasuya, Y. Sasaki, Y. Saito, K. Tohji, and Y. Nishina, Phys. Rev. Lett. **78**, 4434 (1997).
- ²⁰J. Yu, R. K. Kalia, and P. Vashista, J. Chem. Phys. **103**, 6697 (1995); Europhys. Lett. **32**, 43 (1995).
- ²¹M. Menon, E. Ritcher, and K. R. Subbaswamy, J. Chem. Phys. **104**, 5875 (1996).
- ²²Preliminary results have been presented in the short review by P. Ordejón, D. Sánchez-Portal, E. Artacho, and J. M. Soler (unpublished).
- ²³R. A. Jishi, L. Venkataraman, M. S. Dresselhaus, and G. Dresselhaus, Chem. Phys. Lett. **209**, 77 (1993).
- ²⁴M. S. Tang, C. T. Chang, and K. M. Ho, Phys. Rev. B **53**, 979 (1996); J. Phys.: Condens. Matter **4**, 6047 (1992), and references therein.
- ²⁵P. Ordejón, E. Artacho, and J. M. Soler, in *Materials Theory, Simulations, and Parallel Algorithms*, edited by E. Kaxiras *et al.*, MRS Symposia Proceedings No. 408 (Materials Research Society, Pittsburgh, 1996), p. 85; Phys. Rev. B **53**, R10 441 (1996).
- ²⁶W. Kohn and L. J. Sham, Phys. Rev. **140**, 1133 (1965). The exchange-correlation potential is taken from D. M. Ceperly and B. J. Alder, Phys. Rev. Lett. **45**, 566 (1980), as parametrized by J. Perdew and A. Zunger, Phys. Rev. B **23**, 5048 (1981).
- ²⁷R. W. Jansen and O. F. Sankey, Phys. Rev. B **36**, 6520 (1987).
- ²⁸O. F. Sankey and D. J. Niklewski, Phys. Rev. B **40**, 3979 (1989).
- ²⁹D. Sánchez-Portal, E. Artacho, and J. M. Soler, J. Phys.: Condens. Matter **8**, 3859 (1996).
- ³⁰P. Ordejón, D. A. Drabold, R. M. Martin, and M. Grumbach, Phys. Rev. B **51**, 1456 (1995).
- ³¹P. Ordejón, Comput. Mater. Sci. **12**, 157 (1998), and references therein.
- ³²P. Ordejón, D. A. Drabold, R. M. Martin, and S. Itoh, Phys. Rev. Lett. **75**, 1324 (1995).
- ³³W. Frank, C. Elsässer, and M. Fähnle, Phys. Rev. Lett. **74**, 1791 (1995).
- ³⁴Y. Baskin and L. Mayer, Phys. Rev. **100**, 544 (1955).
- ³⁵M. C. Schabel and J. L. Martins, Phys. Rev. B **46**, 7185 (1992).
- ³⁶We have found that the difference between the inequivalent bond lengths is extremely sensitive to the k -point sampling. The behavior shown in Fig. 1(a) has been checked in two ways: (i) by comparing the tube results with the relaxations of a graphene sheet with an identical k -point sampling, and (ii) using more complete k samplings in the tube calculations. In both cases the same behavior as presented in Fig. 1(a) was found when the bond lengths are expressed in units of the corresponding bond distances for graphene calculated with equivalent sampling. The absolute lengths are more difficult to converge, being inverted for the samplings used in Ref. 7.
- ³⁷L. C. Venema, J. W. G. Wildöer, S. J. Tans, J. W. Janssen, L. J. Hinne, T. Tuinstra, L. P. Kouwenhoven, and C. Dekker, Science **283**, 52 (1999); A. Rubio, D. Sánchez-Portal, E. Artacho, P. Ordejón, and J. M. Soler, Phys. Rev. Lett. (to be published).
- ³⁸G. G. Tibbetts, J. Cryst. Growth **66**, 632 (1983).
- ³⁹G. Adams, O. Sankey, J. Page, M. O’Keeffe, and D. Drabold, Science **256**, 1792 (1992).
- ⁴⁰G. Overney, W. Zhong, and D. Tomanek, Z. Phys. D **27**, 93 (1993).
- ⁴¹R. L. Jacobsen *et al.*, Carbon **33**, 1217 (1995); J. D. H. Hughes, *ibid.* **24**, 551 (1986).
- ⁴²O. L. Blakslee, D. G. Proctor, E. J. Seldin, G. B. Spence, and T. Weng, J. Appl. Phys. **41**, 3373 (1970); E. J. Seldin and C. W. Nezbeda, *ibid.* **41**, 3389 (1970).
- ⁴³This data is in agreement with *ab initio* pseudopotential plane-wave calculations of the Poisson ratio in carbon nanotubes. The computed values of 0.151 and 0.180 for the (5,5) and (10,0) nanotubes are in excellent agreement with the present calculations of 0.14 and 0.19, respectively.
- ⁴⁴C. Oshima, T. Aizawa, R. Souda, Y. Ishizawa, and Y. Sumiyoshi, Solid State Commun. **65**, 1601 (1988).
- ⁴⁵P. Pavone, R. Bauer, K. Karch, O. Schütt, S. Vent, W. Windl, D. Strauch, S. Baroni, and S. de Gironcoli, Physica B **219**, 439 (1996).

- ⁴⁶G. Kresse, J. Furthmüller, and J. Hafner, *Europhys. Lett.* **32**, 729 (1995).
- ⁴⁷P. C. Eklund, J. M. Holden, and R. A. Jishi, *Carbon* **33**, 959 (1995); H. Hiura, T. W. Ebbesen, K. Tarigaki, and H. Takahashi, *Chem. Phys. Lett.* **202**, 509 (1993).

- ⁴⁸Y. Miyamoto, M. L. Cohen, and S. G. Louie, *Phys. Rev. B* **52**, 14 971 (1995).
- ⁴⁹A. A. Lucas, P. H. Lambin, and R. E. Smalley, *J. Phys. Chem. Solids* **54**, 587 (1993), and references therein.